

# Beyond Wavelets: Exactness theorems for physical calculations

T.A. Arias and T.D. Engeness

Department of Physics  
Massachusetts Institute of Technology, Cambridge MA 02139, USA

**Abstract.** This paper develops the use of wavelets as a basis set for the solution of physical problems exhibiting behavior over wide-ranges in length scale. In a simple diagrammatic language, this article reviews both the mathematical underpinnings of wavelet theory and the algorithms behind the fast wavelet transform. This article underscores the fact that traditional wavelet bases are fundamentally ill-suited for physical calculations and shows how to go beyond these limitations by the introduction of the new concept of *semicardinality*, which allows basic physical couplings to be computed *exactly* from very sparse information, thereby overcoming the limitations of traditional wavelet bases in the treatment of physical problems. The paper then explores the convergence rate of conjugate gradient solution of the Poisson equation in both *semicardinal* and *lifted* wavelet bases and shows the first solution of the Kohn-Sham equations using a novel variational principle.

## 1 Introduction

Problems in the physical sciences often involve behavior spanning many length scales. Three ingredients, which do not necessarily follow one from the other, are needed to deal effectively with such problems : (1) compact representation of the fluctuations of physical fields over different length scales in different regions of space, (2) economical expression of the physical couplings among such fields, and (3) efficient means for solving the resulting equations. The discussion below gives a very powerful general means for dealing with such problems. Although, the discussion is general, for concreteness we shall consider the calculation of electronic structure of matter, reviewed briefly in Sec. 2, as a prototypical example.

As we shall see in Sec. 3, the central concept underlying wavelet theory, multiresolution analysis, is a very elegant and powerful mathematical tool for providing compact representations, but the expression of the most common physical couplings is very awkward in traditional wavelet bases. Sec. 4 shows how the introduction of a new concept, *semicardinality* provides a means of overcoming this limitation and providing an extremely efficient and, surprisingly, *exact* means of expressing the two most fundamental physical couplings. Finally, Sec. 5 shows extremely efficient methods for solving Poisson's equation and the Kohn-Sham equations within this new framework.

## 2 Electronic structure of matter

### 2.1 Multiscale nature

It is well known that the electronic wave functions in molecular and condensed-matter systems vary much more rapidly near the atomic nuclei than in interatomic regions. In the immediate vicinity of the nucleus and its strong attractive potential, the electrons possess large kinetic energies, as reflected by high spatial frequencies evident in the orbitals. Figure 1 illustrates this behavior, using the carbon atom as an example. The curves in the figure show the Kohn-Sham orbitals of the atom as computed within the local density approximation [1] to density functional theory [2]. The high-frequency “core” region extends only approximately 0.5 bohr radii out from the nucleus, beyond which the variations in the wave functions are quite smooth. Resolving the cusps in the  $s$  states of this atom requires a resolution on the order of 0.03 bohr (corresponding to a plane wave cutoff [3] of nearly 160,000 rydberg). To provide this resolution uniformly throughout the computational cell of these calculations, which is 8 bohr on a side, would require a basis with 16 million coefficients. The vast majority of these basis functions would be wasted as they would serve to provide unnecessarily high resolution outside the core region.

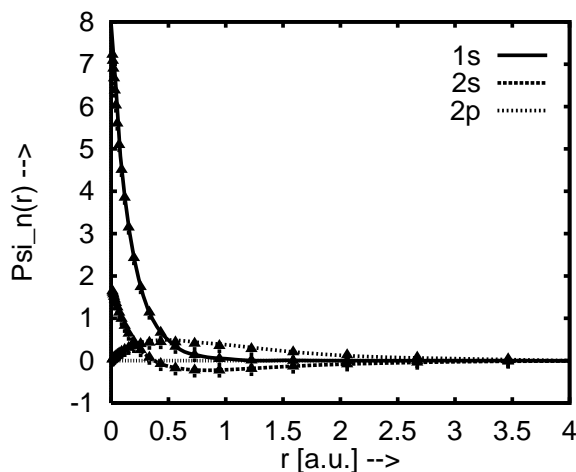


**Fig.1.** Kohn-Sham orbitals of the carbon atom within the local density approximation from standard atomic software (*symbols*) and multiresolution analysis(*curves*) [4]

The issue of multiple length-scales in electronic structure is not new. It has driven the development of a variety of techniques which are now quite mature, including the atomic sphere family of approaches, which uses one type of basis

set inside of a set of spheres organized around the nuclei and another type of basis set outside of the spheres, and the plane wave pseudopotential approach, which replaces the atomic core with an effective potential manufactured to have similar scattering properties. While each of these approaches has had great success, none is systematically improvable to complete convergence in a simple, practical manner, and each requires great care and expertise in the selection and construction of the atomic spheres or in the development of appropriate pseudopotentials. As a result, a general method is still needed to obtain unambiguous results of sufficient accuracy to permit direct and systematic study of the relative accuracy of competing density functionals and alternate theories of electronic structure. This situation calls for precisely the capabilities of multiresolution analysis, which holds the promise of at last enabling the systematic evaluation of different theories of electronic structure at high precision.

## 2.2 Electronic Structure

Throughout this paper, we shall work within the local density approximation (LDA) to density functional theory[1]. A novel way to express the Kohn-Sham equations within this approximation, first introduced in [5], is through the following variational principle (in atomic units  $\hbar = m = e = 1$ ),

$$0 = \delta \mathcal{L}_{LDA} = \delta \int \left[ \sum_i f_i \frac{1}{2} |\nabla \psi_i(\mathbf{r})|^2 + V_{\text{nuc}}(\mathbf{r}) n(\mathbf{r}) + \epsilon^{\text{xc}}(n(\mathbf{r})) n(\mathbf{r}) + \phi(\mathbf{r}) n(\mathbf{r}) - \frac{1}{8\pi} |\nabla \phi(\mathbf{r})|^2 \right] d^3 \mathbf{r}. \quad (1)$$

Here, the minimization is over orthonormal sets of Kohn-Sham orbitals  $\{\psi_i(\mathbf{r})\}$  and the electrostatic (Hartree) potential  $\phi(r)$  of the electrons,  $V_{\text{nuc}}(\mathbf{r})$  is the potential of the nuclei, the electron density is defined as

$$n(r) \equiv \sum_i f_i |\psi_i(r)|^2, \quad (2)$$

the  $f_i$  are the occupancies of the Kohn-Sham orbitals, and  $\epsilon^{\text{xc}}(n)$  is the exchange-correlation energy per electron in a uniform electron gas of density  $n$ , a highly non-linear function. The advantage of this new variational principle is that it does not involve the traditional long-range Hartree integral,

$$E_{\text{Hartree}} = \int d^3 \mathbf{r} d^3 \mathbf{r}' \frac{n(\mathbf{r}) n(\mathbf{r}')}{|\mathbf{r} - \mathbf{r}'|}. \quad (3)$$

It thus expresses the physics of electronic structure in terms of two simple types of coupling: (1) purely local, but possibly non-linear couplings, and (2) semi-local quadratic couplings among the fields through differential operators. Any successful approach to electronic structure and other physical problems

must specify how to deal effectively with these two forms of coupling. This new variational principle also leads to a novel solution of the Kohn-Sham equations (Sec. 5.2).

### 3 Compact representation of fields

#### 3.1 Two-scale decomposition

Figure 2a illustrates the concept of *two-scale decomposition* for functions in one dimension. The first row shows a basis set capable of describing functions which fluctuate on length scales greater than the unit distance. This basis consists of copies of a single function  $s(x)$ , illustrated as piece-wise linear functions of triangular appearance in the figure, translated onto each integer point  $n$  along the real axis. The linear space of functions which may be written in terms of this basis is called  $V_0$ . The simplest way to double the resolution of this basis is to simply “compress” it by a factor of two, reducing the horizontal scale of both the functions and of the lattice of points on which they sit, as sketched in the final row of the figure. The space spanned by this finer basis is called  $V_1$ . Two-scale decomposition builds upon the original coarser basis for  $V_0$  to produce a basis equivalent to the finer basis for  $V_1$  by adding a new set of basis functions  $d(x)$  called *detail functions*, or sometimes *wavelets*. The figure shows these functions along the center row. The *detail space*, denoted  $W_1$ , is the space of functions which may be written solely in terms of these detail functions. For the combined basis to be equivalent to the “compressed” basis, every function in  $V_1$  must be expressible as a sum of one function in  $V_0$  and one in  $W_1$ . In the language of linear subspaces,  $V_0 \oplus W_1 = V_1$ .

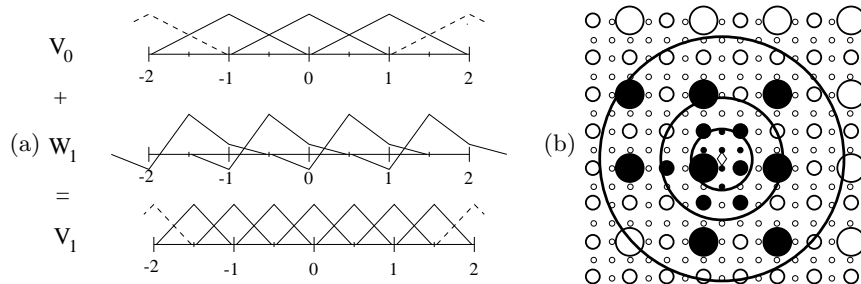


**Fig. 2.** Two-scale decomposition. (a) One dimension. (b) Multiple dimensions. Coarse grid (*larger circles*), detail points of finer grids (*smaller circles*), atomic nucleus (*diamond*), spheres of resolution (*large circles*), surviving basis functions (*filled circles*)

This condition determines much about the form of the basis functions. First, the spaces  $V_0 \oplus W_1$  and  $V_1$  must have the same dimension, and thus

equal numbers of basis functions, so that there must be one detail function for each point which appears in the finer lattice but not in the original coarse lattice. (In the figure, these are the odd half-integer points.) Next the basis functions for both  $V_0$  and  $W_1$  must also be in the space  $V_1$ . This specifies a profound restriction on the original basis function, that it may be written exactly in terms of compressed and translated versions of itself,

$$s(x) = \sum_n c_n s(2x - n). \quad (4)$$

This relation which connects the same basis functions on two different scales is known as the *two-scale relation*, the coefficients  $c_n$  are known as the *two-scale coefficients*, and the functions satisfying this condition are known as *scaling functions*. (For a detailed discussion, see [6].) Finally,  $V_0 \oplus W_1 = V_1$  implies that the detail functions are simply linear combinations of the compressed basis functions,

$$d(x) = \sum_n d_n s(2x - n), \quad (5)$$

where the coefficients  $d_n$  are known as the *detail coefficients*.

The preceding conditions ensure that  $V_0 \oplus W_1 \subset V_1$ . To show that the combined and the finer spaces are indeed equal, one must also show that all functions in  $V_1$  may be written in terms of a linear combination of coarse scaling functions and detail functions. In as much as the two bases contain equal numbers of functions and all functions in either space are linear combinations of finer scaling functions, this amounts to showing that a particular linear system of equations involving the two-scale and detail coefficients always has a solution. There is therefore a certain determinant which must be verified to have non-zero value [7, Theorem 5.16], a condition easily satisfied in practice.

### 3.2 Multiresolution analysis

To go beyond two-scale decomposition, we note that starting from  $V_0$ , one may produce an entire class of bases of successively higher resolution by reducing the scale of space by successive powers of two. This process defines a sequence of lattices  $C_0, \dots, C_N, \dots$ , associated with a sequence of bases of increasing resolution,  $V_0, \dots, V_N, \dots$ . Simply changing the horizontal scale in Figure 2a and the variable  $x$  in Eqs. (4,5) by a factor of  $2^Q$  gives the prescription for defining the detail space  $W_{Q+1}$  which gives  $V_Q + W_{Q+1} = V_{Q+1}$ : the basis for  $W_{Q+1}$  simply consists of detail functions compressed by a factor of  $2^Q$ ,  $d(2^Q x)$ , centered on the points  $D_{Q+1} \equiv C_{Q+1} - C_Q$  which appear in  $C_{Q+1}$  but not  $C_Q$ . Finally, iterative application of two-scale decomposition can produce spaces  $V_N$  of *arbitrarily* fine high resolution,  $V_N = V_0 \oplus W_1 \dots \oplus W_N$ , and thus express the entire Hilbert space of functions in one dimension in terms of a basis of hierarchical levels of detail.

These ideas apply equally well in multiple dimensions, as Figure 2b illustrates. Again, the multiresolution analysis begins with a coarse lattice  $C_0$  on which are centered the coarse scaling functions (large circles in the figure). Then, to double the resolution, detail functions appear on the points of  $D_1$  (intermediate circles in the figure), and to double the resolution yet again, detail functions compressed by a factor of two are added to the points of  $D_2$  (small circles in the figure).

Although such a basis separates functions into contributions on different scales, the final basis still consists of one basis function for each point on the finest scale grid, thus requiring many coefficients to represent physical fields. Figure 2b illustrates how to reduce the size of the basis without significant loss of information. Only the immediate vicinity of the nuclei requires the very highest level of resolution  $N$ , and successively lower levels of resolution are required as we move outward from the nuclei. Therefore, about each nucleus we draw a set of successively inscribed spheres of appropriate radii for the scales  $0 \dots N$  chosen to cut off functions with coefficients below a predetermined tolerance, and we keep in the basis only those functions of a given scale which fall within the corresponding sphere (filled circles in the figure). We refer to this process as *restriction*. This process may be carried out adaptively if desired[8].

Such restriction maintains a description equivalent, within the predetermined tolerance, to the full basis  $V_N$  and thus the underlying *uniform* basis on the finest scale. In contrast to finite element approaches, the basis functions of a multiresolution analysis constructed this way do not move with the atoms. The only effect of the motion of the atoms is to turn on or turn off basis functions whose coefficients are below the selected tolerance.

Figure 1 shows two sets of results whose comparison demonstrates how well this approach compacts the representation of electronic wave functions. The triangular points in the plot display the results of an essentially exact calculation within the local density approximation, obtained by exploiting the spherical symmetry of the atom. The curves in the figure show that the results obtained from a full, three dimensional calculation using a restricted multiresolution analysis are nearly indistinguishable from the exact results. Yet, rather than requiring a coefficient for each point of the effective grid of 16 million points, the results in the figure come from a restricted basis with six levels of refinement giving a total of only 2,500 functions, compacting the representation by over three orders of magnitude!

## 4 Expression of physical couplings

### 4.1 Non-linear, local couplings

Figure 3a gives an explicit, diagrammatic representation of the calculation of a non-linear, local coupling among physical fields. Although the procedure is completely general, as an example we consider the computation of

the exchange-correlation energy per particle  $\epsilon^{xc}(\mathbf{r})$  in terms of the electronic wave functions. The calculation begins at the top of the figure with the multiscale expansion coefficients  $C_\alpha$  for the electronic wave functions and ends at the bottom with the corresponding multiscale coefficients for the exchange-correlation field. The circles represent values during the course of the calculation, and the arrows represent mathematical operations which first multiply the value at the base of the arrow by a coefficient specific to the arrow and then accumulate the result onto the value at the head of the arrow. In the first and final rows, the large circles represent the expansion coefficients for the coarse scaling functions in the multiresolution analysis, the intermediate circles are those for the detail functions and the small circles for the finer detail functions.

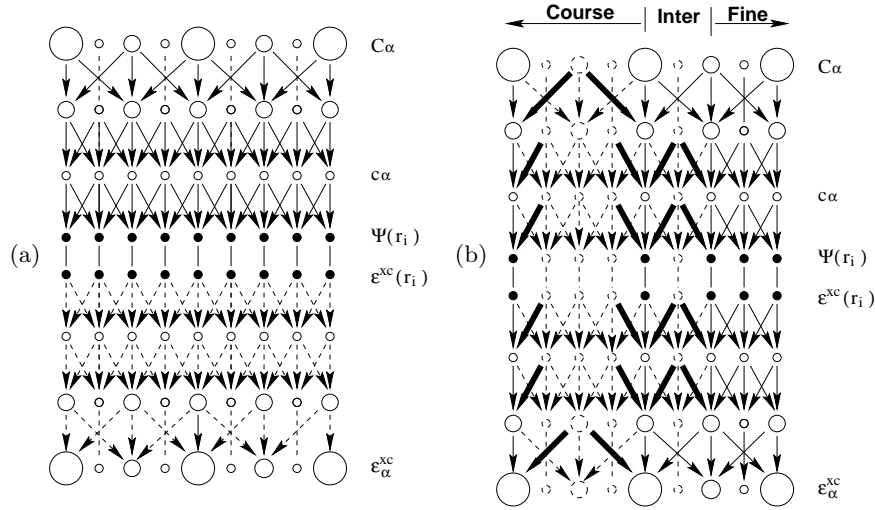


**Fig. 3.** Calculation of the exchange-correlation field. (a) Unrestricted multiresolution analysis. (b) Restricted multiresolution analysis. Coarse-scale expansion coefficients (*large circles*), intermediate-scale coefficients (*mid-sized circles*), fine-scale coefficients (*small circles*), function values (*filled points*), multiply-accumulate operations (*arrows*)

The calculation proceeds in three phases. The first, *forward phase* (first through fourth rows of the figure) determines the values of the fields on a set of points in space  $\mathbf{r}_i$  by first finding the equivalent expansion coefficients  $c_\alpha$  for the underlying basis of finest-scale scaling functions and then using these coefficients to compute the real-space values. The first stage of this process (first through third rows) is the fast wavelet transform, explained below in Sec. 4.2. The second stage (third through fourth rows) involves taking the single-scale expansion coefficients  $c_\alpha$  (small circles), multiplying by the values of the basis function on the points  $\mathbf{r}_i$  and accumulating the result onto those

points (filled circles), as represented by the arrows. In the second, *coupling* phase (fourth through fifth rows), the known values at the points  $\mathbf{r}_i$  are combined in the purely local, non-linear fashion prescribed by the coupling. In this example, at each point  $\mathbf{r}_i$  we take the square magnitude  $|\psi(\mathbf{r}_i)|^2$  of each wave function, add the results together to compute the charge density  $n(\mathbf{r}_i)$  and then evaluate the non-linear function  $\epsilon^{\text{xc}}(n(\mathbf{r}_i))$ . The figure represents this independent, point-by-point operation as a set of simple vertical lines. Finally, once the non-linear field is known at all points in space, for the third, *inverse phase* of the calculation (fifth through final row), one inverts the first stage of the procedure and determines the multiscale expansion coefficients for the field in terms of its real-space values by inverting each stage of the forward phase in reverse sequence. Inspection of each of the forward stages reveals that it is a convolution, the inverse of which is another convolution, which may be implemented in the same form but with the arrows potentially carrying different coefficients. (For a more detailed discussion, we refer the reader to [6].)

## 4.2 Fast wavelet transform

The upper three rows of Figure 3a illustrate the *fast wavelet transform*, which computes the single-scale expansion coefficients  $c_\alpha$  of a function from its multiscale expansion coefficients  $C_\alpha$ . The basic strategy is for each stage of the calculation to give an equivalent expansion of the original function but in terms of a multiresolution analysis involving one fewer scale, proceeding in this way until the single-scale representation is reached.

The upper two rows of the figure illustrate the first such stage. As Eqs. (4,5) prescribe, each coarse scaling function and detail function of the original multiresolution analysis (large and intermediate circles of the first row) may be expanded exactly in terms of the intermediate scaling functions (larger circles of the second row). Thus, the arrows which multiply the values carried by the two sets of larger circles on the first row by the corresponding two-scale  $c_n$  or detail  $d_n$  coefficient and accumulate the result onto the scaling functions of the next scale compute the required equivalent expansion of the original function in a multiresolution analysis of one fewer scale. The coefficients of the finer detail functions play no role in this process, and so are simply copied to the second row as indicated by dashed lines in the figure. Each stage proceeds exactly in this manner.

The number of floating point operations in this transform varies strictly linearly with the number of points in the grid, and thus scales superiorly even to the fast Fourier transform. Typically, the fast wavelet transform requires only approximately 60 floating point operations per grid point. This efficiency, however, is quickly lost when using a restricted multiresolution analysis.



### 4.3 Impact of restriction

Figure 3b illustrates the impact of restricting the multiresolution analysis on the calculation of local, non-linear couplings. The basis functions indicated by dashed circles are to be removed from the basis, providing a coarse resolution on the left, an intermediate level of resolution near the center, and a fine resolution on the right. The arrows show the same flow of information as before, but now are drawn to convey the impact of the restriction on the progress of the calculation. Under the restriction, there are three distinct types of information flow. The dashed arrows carry information onto values which have been restricted from the basis, and so we may ignore them in the calculation. The thin, solid arrows carry information from functions in our basis to other functions in our basis and represent calculations which we must perform. Finally, the thick, solid arrows are problematic and carry information from functions restricted from the basis onto function maintained therein and thus have the potential to corrupt the final results of the calculation.

In practice, the thick arrows in the forward phase of the transform (upper portion of the figure) do not corrupt the calculation significantly because the expansion coefficients at their base were determined to be small when the restriction for the basis was chosen. The difficulty is in lower portions of the figure, where the arrows carry not expansion coefficients, but *real-space values* of the fields, which need not be small. Tracing back the flow from these arrows, it is evident that to properly compute the final coarse expansion coefficients ultimately requires computing the non-linear coupling on all points of the finest grid.

In terms of computational expense, this sacrifices much of the benefit of the multiresolution analysis. Returning to the example of the calculation of the carbon atom, although the wavelet transforms require only about 60 operations per grid point and only 2,500 basis functions were required in the basis, the need to evaluate fields on the finest scale of 16 million points requires the expenditure of 400,000 floating point operations per basis function. A pseudopotential calculation (at 44 rydberg cutoff) in the same cell also requires approximately 2,500 basis functions, but, through the use of the fast Fourier transform, requires only approximately 400 floating point operations per basis function. Without a major advance, the computational expense of representing the physics of the core in a multiresolution analysis thus would require such a computational cost as to relegate such calculations to a very special niche where systematic results are needed very badly.

Our strategy to make the wavelet transform competitive in *restricted* multiresolution analyses is to find multiresolution analyses which eliminate all information flow along the thick arrows in Figure 3b. We could then compute the results of the transform by simply ignoring the values associated with the dashed circles in the figure so that the transforms may be computed with only approximately 60 floating point operations per *basis function*, less effort than even the fast Fourier transform. Profoundly, without the thick

diagonal arrows carrying information from finer scale functions onto neighboring coarser functions, the results obtained in a restricted multiresolution analysis of finite, variable resolution then would be identical to *exact* results obtained by beginning with full knowledge of the physical fields, transforming onto a grid of arbitrarily fine resolution, computing the interaction, and transforming the result back! We refer to this property as *exactness*.

#### 4.4 Exactness through semicardinality

We now show a multiresolution analysis which gives rise to such exact results for non-linear, local couplings. For the scaling functions, we draw inspiration from finite-element theory and consider *cardinal* functions, those with zero value on all grid points except for one, where their value is normalized to unity. As Figure 4a illustrates, the nodal properties of a single-scale basis of cardinal functions ensure that the expansion coefficients of a function and its real-space values on the grid are equal. For the two-scale relation (Figure 4b), this implies that the two-scale coefficients are simply the values of the scaling function sampled on a grid of half-spacing so that the two-scale coefficients never carry information from a coarse function onto points associated with other coarse functions, an important condition in obtaining exactness.

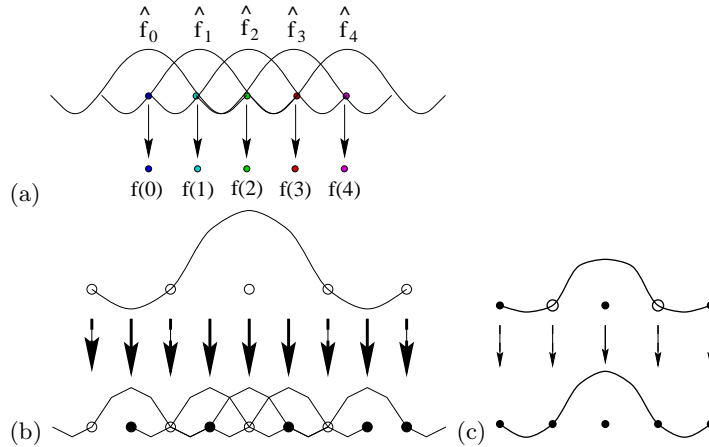


**Fig. 4.** Semicardinal multiresolution analysis. (a) Underlying uniform basis of scaling functions. (b) Two-scale decomposition of scaling functions, (c) decomposition of detail functions. Zero coefficients (*dashed arrows*)

For the detail functions, we impose the condition that they be zero on the points of the finer scale whose details they carry (Figure 4c). One cannot restrict the detail functions to be appear cardinal on the points of the finer scales because then they would become  $\delta$ -like functions. The coarser-looking, “one-way” form of the cardinality of the basis we construct in this way we

refer to as *semicardinality*. As Figure 4c illustrates, *semicardinality* implies that all detail coefficients  $d_n$  but one are zero, so that the detail functions are simply finer-scale scaling functions, a condition not exhibited in traditional wavelet bases.

An immediate benefit of the cardinality of the scaling functions in a semi-cardinal basis is that once the forward wavelet transform is complete (Figure 5a), the expansion coefficients on the finest scale are just the values of the function on the finest grid and the forward phase of the calculation is complete. The nodal conditions in the two-scale and detail coefficient sequences make calculation of the inverse phase of the calculation simple as well. Because at each stage of the forward transform (Figure 5a) the information flowing out from the scaling functions carries vertically downward without change, in the stages of the inverse transform (Figure 5a) the final values for the coarser functions may simply be copied again vertically without change. The information flowing out from the detail functions in the forward transform flows vertically, but is met by information flowing diagonally from the scaling functions. Therefore, in the inverse transform, the final values for the detail functions may be copied vertically but met with diagonal information flow of the opposite sign. Note that the pattern of information flow is identical for the corresponding stages of the two transforms. The only change is reversal of the signs of the diagonal arrows.

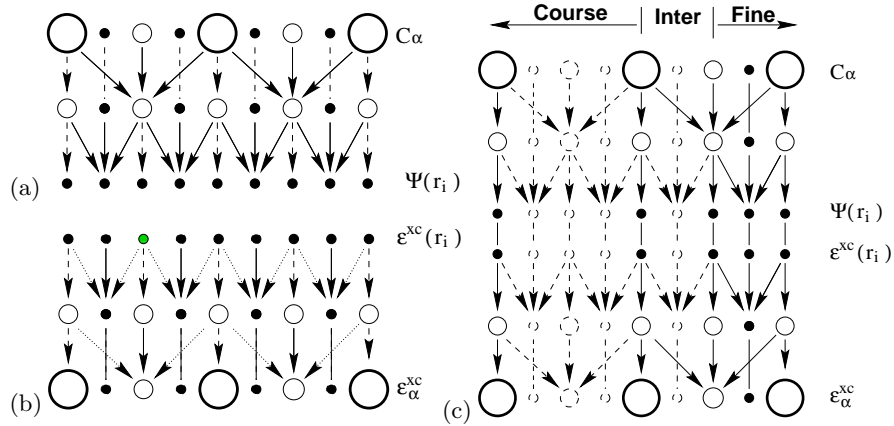


**Fig. 5.** Calculation of non-linear, local interactions in semicardinal multiresolution analyses. (a) Forward transform. (b) Inverse transform. (c) Complete calculation in restricted basis

Figure 5c shows the computation of a non-linear, local interaction in a restricted *semicardinal* multiresolution analyses. The expression of these interactions involves no corrupting information flow and is now *exact* and may be computed more efficiently than with the fast Fourier transform! Similar

results hold in semicardinal bases for the economical expression of couplings through differential operators. One also may compute these interactions *exactly* while working with only those functions that survive a restriction[6].

## 5 Efficient solutions

### 5.1 Poisson’s equation

To solve Poisson’s equation, we use the variational principle of minimizing the electrostatic (Hartree) energy. When the potential  $\phi(\mathbf{r})$  is expanded in a basis, the result is a linear system of equations involving the Galerkin representation for the Laplacian operator. In this section, we focus on the convergence rate of conjugate gradient techniques in solving the resulting equation.

As our example, we compute the electrostatic potential of the carbon atom as a full three-dimensional problem. The basis we employ consists of 12 levels of refinement, each consisting a cubic array of approximately  $24^3$  detail functions. (We use cubic refinement regions as a matter of computational expediency.) The total number of functions in the basis is approximately 200,000, and the basis represents a range in length scale and thus condition number of the Laplacian operator in excess of  $2^{12}$  and  $2^{24} \approx 16 \times 10^6$ , respectively. Under these conditions, one would expect conjugate gradients to require tens of thousands of applications of the operator to solve the equation.

Figure 6 shows the convergence of conjugate gradient methods for solving Poisson’s equation with different preconditioners: “diagonal” multiplies the residual by the inverses of the diagonal matrix elements of the Laplacian, “block-diagonal” uses Fourier techniques to invert the diagonal sub-blocks of the Laplacian matrix which connect functions of the same scale with each other, and “multi-level” uses special techniques to invert the upper and lower triangular blocks of the Laplacian matrix connecting functions to functions of only higher or lower scales, respectively. These three sets of calculations were carried out using a semicardinal bases of third order. The data labeled “lift” are results for simple diagonal preconditioning of the Galerkin representation of the Laplacian in a second type of basis, a basis of third-order *lifted wavelets* of the Sweldens construction[9]. The vertical axis of the figure displays the square-magnitude of the residual vector, which varies linearly with the error in the computation of the electrostatic energy because the calculation is variational. To accurately reflect the varying complexity of the different preconditioners, the horizontal axis indicates net computational time in “work units” (WU) defined to be the computational effort of applying the Laplacian operator in the semicardinal basis. For the simple preconditioners, the horizontal axis closely corresponds to number of iterations.

The upshot of the figure is that in these multiresolution bases, conjugate gradients determines the electrostatic energy to within machine precision in only about 100 iterations, three orders of magnitude better than expected!

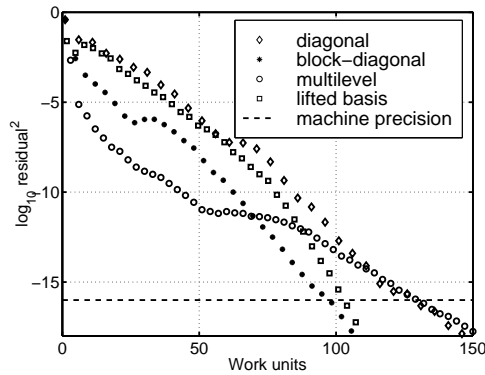


**Fig. 6.** Solution of Poisson’s equation. Convergence of square magnitude of residual vector with various preconditioners in semicardinal and lifted multiresolution bases

(The first reported calculations which uses this basis with the diagonal preconditioner appear in [4].) These very high convergence rates,  $\sim 0.15$  digits/WU, reflect the fact that the semicardinal basis reorganizes the structure of the operator in such a way to enhance its diagonal structure. The most successful approach is the block-diagonal preconditioner. Whereas the multilevel preconditioner gives a dramatic improvement in the number of iterations required to solve the equation, these benefits are outweighed by its computational cost.

In regards to calculation with lifted wavelets, it has been suggested recently that the non-zero integral of the detail functions of a semicardinal basis would create a bottleneck in the solution of Poisson’s equation and that, instead, one should use a lifted interpolant basis in which the low order moments of the detail functions vanish[10]. Figure 6b (*squares*) shows that although there is a modest improvement in the convergence at the final stages of the calculation, there is no great advantage in the solution of Poisson’s equation from the properties of the lifted basis.

Finally, we consider the impact of problem size on the convergence rate of the electrostatic energy as we increase the level of resolution and the spatial extent of the refinement regions (Figures 7a and 7b, respectively). Figure 7a shows that going as far as 24 levels of refinement, the convergence rate of the diagonal and block-diagonal preconditioners does not degrade appreciably despite the condition number of the Laplacian operator now reaching  $2^{48} \sim 280$  trillion. This finest level places 1,000 grid points across the extent of the carbon nucleus, more than sufficient to resolve the individual quarks within the nucleons. Figure 7b explores the behavior of convergence rate as we increase the linear extent of the refinement regions up to about two times the size expected to be relevant in the calculation of electronic structure. Although the diagonal preconditioner degrades somewhat over this range, the block-diagonal conditioner maintains a nearly constant convergence rate of

0.16 digits/WU for the electrostatic energy. The stability of these convergence rates strongly suggests that, regardless of problem size, a fixed number of approximately 100 iterations are required to solve Poisson's equation to a given tolerance.

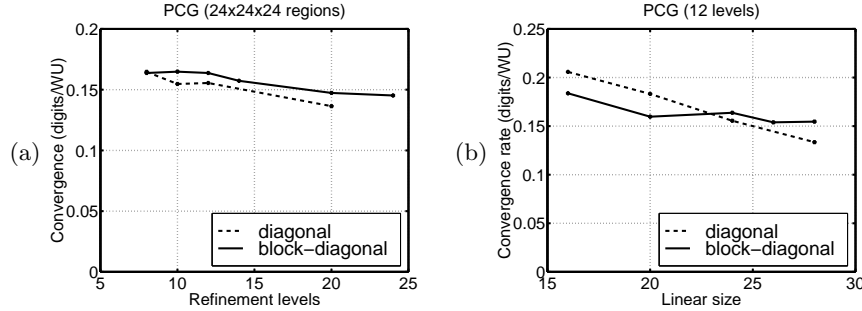


**Fig. 7.** Behavior of convergence rate in solution of Poisson's equation in semicardinal bases. (a) Variation with number of refinement regions, each of size  $24^3$ . (b) Variation with spatial extent of refinement regions

## 5.2 Kohn-Sham equations

As we saw in the preceding section, the solution of Poisson's equation in semicardinal bases is surprisingly efficient, but still requires on the order of one hundred iterations. This is particularly burdensome in the calculation of electronic structure, where in traditional formulations the Poisson equation must be solved at each step in the minimization of the Kohn-Sham energy functional. We propose instead to search directly for the stationary point of the Lagrangian functional (1). From the signs of the semi-local couplings, it is clear that the stationary point of the Lagrangian functional is a minimum with respect to the electronic wave function fields  $\{\psi_i(\mathbf{r})\}$  and a maximum with respect to the electrostatic potential field  $\phi(\mathbf{r})$ . Although we are searching for a saddle point, our proposed approach is analogous to iterative conjugate gradient minimization but with a few key differences. Each iteration begins at a state point  $(\{\psi_i(\mathbf{r})\}, \phi(\mathbf{r}))$ , but, rather than searching along the downhill-gradient direction  $(-\nabla_{\psi}\mathcal{L}, -\nabla_{\phi}\mathcal{L})$ , we search along the direction  $\mathbf{d} \equiv (-\nabla_{\psi}\mathcal{L}, \nabla_{\phi}\mathcal{L})$ , which is downhill for the electrons and uphill for the electrostatic potential. Next, rather than searching to the point where the functional becomes stationary along the line defined by  $\mathbf{d}$ , we search for the point where the next search direction computed in this same way becomes perpendicular to  $\mathbf{d}$ .

For the beryllium atom, Figure 8 compares the convergence of this new approach with the traditional approach of applying preconditioned conjugate gradients to minimize the energy functional. The horizontal axis measures

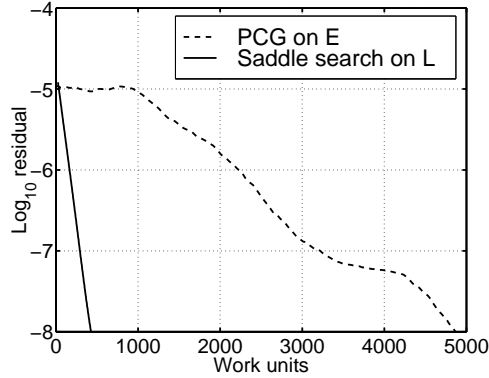


**Fig. 8.** Comparison of energy and Lagrangian functional solutions to Kohn-Sham equations of density functional theory

computational in work units representing the cost of the application of the Laplacian operator. The figure shows that the computational savings from not having to solve Poisson's equation at each iteration makes the Lagrangian approach a full order of magnitude more efficient than the traditional approach based upon minimization of the energy functional.

## References

1. W. Kohn and L. J. Sham. Self-consistent equations including exchange and correlation effects. *Phys. Rev.*, 140:A1133, 1965.
2. P. Hohenberg and W. Kohn. Inhomogeneous electron gas. *Phys. Rev.*, 136:B864, 1964.
3. M.C. Payne, M.P. Teter, D.C. Allan, T.A. Arias, and J.D. Joannopoulos. Iterative minimization techniques for *ab initio* total energy calculations: molecular dynamics and conjugate gradients. *Rev. Mod. Phys.*, 64:1045, 1992.
4. T.A. Arias, K.J. Cho, Pui Lam, and M.P. Teter. Wavelet transform representation of the electronic structure of materials. In Rajiv K. Kalia and Priya Vashishta, editors, *Proceedings of the '94 Mardi Gras Conference: Toward Teraflop Computing and New Grand Challenge Applications*, page 23, Commack New York, 1995. Nova Science Publishers.
5. R.A. Lippert, T.A. Arias, and A. Edelman. Multiscale computation with interpolating wavelets. *J. Comput. Phys.*, 140:278, 1998.
6. T.A. Arias. Multiresolution analysis of electronic structure: semicardinal and orthogonal wavelet bases. *Rev. Mod. Phys.*, 71:267, 1999.
7. C.K. Chui. *An Introduction to Wavelets*. Academic Press, Boston, 1992.
8. C.J. Tymczak and Xiao-Qian Wang. Orthonormal wavelet bases for quantum molecular dynamics. *Phys. Rev. Lett.*, 78:3654, 1997.
9. W. Sweldens. The lifting scheme: A custom-design construction of biorthogonal wavelets. *Appl. Comput. Harm. Anal.*, 3:186, 1996.
10. S. Goedecker and O.V. Ivanov. Linear scaling solution of the coulomb problem using wavelets. *Solid State Commun.*, 105:665, 1998.